

Seamless Handover of Satellite Tracking Using Geographic Aiding

Osechas, O.; Kim, K.J.; Parsons, K.

TR2015-116 September 2015

Abstract

In high-speed terrestrial vehicles, such as passenger or freight trains, moving through a cluttered environment means intermittent availability of navigation satellite signals. This paper presents a method for seamlessly handing over signal tracking from one satellite receiver to another, when both are mounted on the same train. For this purpose the paper looks at the tracking loop in a typical satellite navigation receiver and proposes ways of computing estimates of code phase and carrier frequency to initialize tracking. We test a proof-of concept implementation of the method in simulation. The tests demonstrate the technical feasibility of seamless handover of satellite tracking between navigation satellite receivers.

2015 ION-GNSS+

This work may not be copied or reproduced in whole or in part for any commercial purpose. Permission to copy in whole or in part without payment of fee is granted for nonprofit educational and research purposes provided that all such whole or partial copies include the following: a notice that such copying is by permission of Mitsubishi Electric Research Laboratories, Inc.; an acknowledgment of the authors and individual contributions to the work; and all applicable portions of the copyright notice. Copying, reproduction, or republishing for any other purpose shall require a license with payment of fee to Mitsubishi Electric Research Laboratories, Inc. All rights reserved.

Seamless Handover of Satellite Tracking Using Geographic Aiding

Okuary Osechas*

German Aerospace Center (DLR), Oberpfaffenhofen, Germany

Kyeong Jin Kim and Kieran Parsons

Mitsubishi Electric Research Lab (MERL), Cambridge, MA

Abstract

In high-speed terrestrial vehicles, such as passenger or freight trains, moving through a cluttered environment means intermittent availability of navigation satellite signals. This paper presents a method for seamlessly handing over signal tracking from one satellite receiver to another, when both are mounted on the same train. For this purpose the paper looks at the tracking loop in a typical satellite navigation receiver and proposes ways of computing estimates of code phase and carrier frequency to initialize tracking. We test a proof-of-concept implementation of the method in simulation. The tests demonstrate the technical feasibility of seamless handover of satellite tracking between navigation satellite receivers.

Introduction

The acquisition phase on a conventional Global Navigation Satellite System (GNSS) receiver consists of a time-consuming search of the delay-frequency space. Trains moving at high speeds through cluttered terrestrial environments are at risk of losing track of GNSS signals and re-acquisition of a lost signal means that signal is unavailable to the GNSS receiver on the train.

In the situation depicted in Figure 1 the train is able to maintain lock on the shaded satellite, as long as any of its receivers has lock on it at any given epoch.

To acquire the signal the receiver must identify the frequency at which the signal is arriving, and its pseudo-random noise (PRN) code phase. For each satellite, the receiver correlates the composite

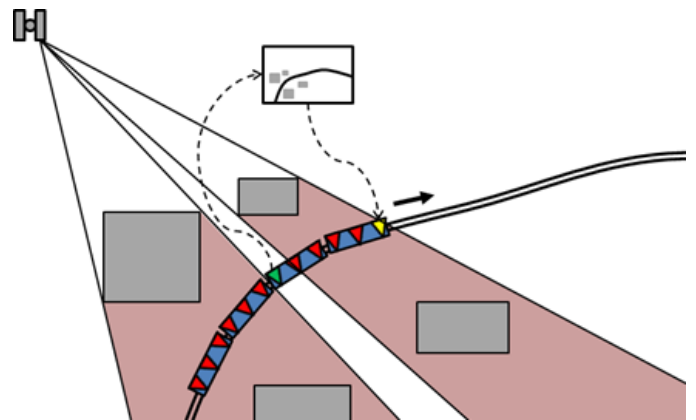


Figure 1: Seamless handover of tracking would allow a train, equipped with multiple GNSS receivers, to maintain continuous lock on GNSS signals in more complex situations than a conventional receiver might. In the situation depicted here, the leading receiver is about to exit the shaded region, while the only functional receiver (marked green) is about to lose lock in the next epoch. Seamless handover of signal tracking from the green receiver to the yellow receiver can provide a continuous position solution throughout this entire situation.

signal, which contains the signals from all visible satellites, with each PRN over various signal delays and Doppler frequencies [1]. The combination of delay and frequency that yields the highest correlation is used to initialize the tracking loop, which is typically composed of a combination of a delay-lock loop (DLL) and a phase-lock loop (PLL) [2].

Acquisition aiding typically consists of using external information to predict the expected code phase and carrier frequency for a particular PRN. Many different

*The work of O. Osechas was done while he was a Post-Doctoral Researcher at MERL.

aiding principles exist [3], but they are usually based on estimating train position or velocity using external signals. The work described in this paper focuses on leveraging the geographic constraints typical of railroad vehicles, where the trajectory of a GNSS receiver can be predicted with sufficient accuracy.

In this paper we discuss two methods that predict code phase and carrier frequency of the signal that is to be acquired, based on geographic and other aiding information. The first method requires a single receiver, but detailed modeling of the code phase; on the other hand, the second method requires a less accurate modeling of the code phase and, instead, relies on a second GNSS receiver to compute the code phase estimate. In this paper we present arguments that support the feasibility of the first method, while a proof of concept for the second method remains an item for future work.

Background: GNSS Signal Tracking

Tracking the signal from each visible GNSS satellite is essential in measuring the distance to that satellite. Tracking consists of estimating over time the code delay and carrier frequency of the detected satellite signal. For this purpose the incoming composite signal is passed through a tracking loop that consists of a PLL and a DLL, as seen in Figure 2. In this design the PLL estimates the signal frequency over time, while the DLL estimates the code phase of the signal; in order to achieve steady tracking, the values for code phase (Φ) and carrier frequency (f) set the initial conditions for the correct operation of the tracking loop. The process is said to acquire, for each satellite, estimates of Φ and f from the incoming composite GNSS signal; these acquired quantities are then used to initialize the tracking loop that provides continuing measurements for Φ and f .

Trade-off in Bandwidth

In designing both, the PLL and the DLL, setting the noise bandwidth (B_L) also sets the dynamics of the tracking loop. In particular, the choice of B_L directly affects the settling time of the tracking loop, as discussed in [1]. Note that it is frequent practice in GNSS receivers to fix the damping of the PLL and DLL to 0.7. The time it takes the system response to reach the fraction $1 - q$ of the final value is defined as the settling time T_S :

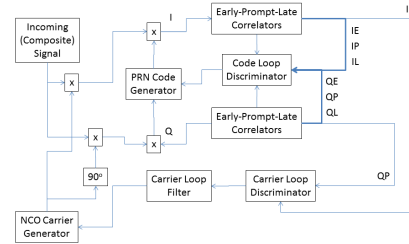


Figure 2: The tracking loop in a typical GNSS receiver, consistent with [1]. The acquisition process sets the initial conditions for the two loop filters: the code phase estimate ($\hat{\Phi}$) initializes the code loop filter, while carrier frequency estimate (\hat{f}) initializes the carrier loop filter.

$$T_S = \ln(q) \frac{(4\zeta^2 + 1)}{8\zeta^2 B_L} \quad (1)$$

In practical terms this means that a PLL with a smaller bandwidth will retain lock for longer than one with a greater bandwidth, after the signal becomes unavailable. On the other hand, it will also take longer to re-acquire lock, for a given initialization error. Additionally, a smaller bandwidth implies a less noisy signal, than a greater bandwidth. Figure 3 shows how the choice of PLL bandwidth affects the rejection of an acquisition error, as well as noise suppression.

In a modern GNSS receiver, the noise bandwidth of the PLL and DLL are adaptive, for example gradually reducing the bandwidth in steps [4]. In that case, seamless handover would enable the receiver to skip the intermediate bandwidths steps and jump right into the regime with the most narrow band widths. This would reduce the ranging noise during the transition period, during which the signal is acquired and the tracking loop uses wider noise bandwidths.

Exploiting Geographic Information

One fundamental way in which railway systems differ from other modes of transportation is the fact that they run on rigid tracks. This kinematic constraint can be leveraged for navigation purposes if the layout of the constraint is known. In such a case the navigation problem becomes one-dimensional, as a single variable describes the along-track position that

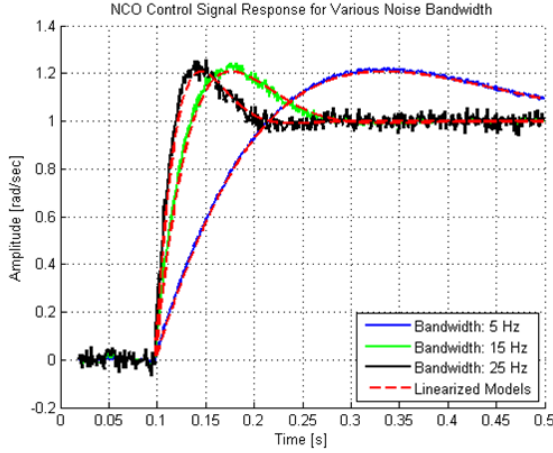


Figure 3: Three different PLLs with different noise bandwidths reject noise in different ways. They also respond differently to initial conditions (i.e. errors in acquisition). The response to an initial condition is modeled for each bandwidth, as in (1). The plot shows how a faster settling time (black signal: BW = 25 Hz) leads to a noisier output than a slower settling time (blue signal: BW = 5 Hz).

uniquely maps into three-dimensional space.

Tools exist to survey tracks with millimeter accuracy [5]. Whether or not it is current practice, a desire exists to achieve this kind of performance [6], and it is certainly reasonable to assume that railway users will be able to access this information in real time [7].

Under these conditions the position of one end of the train (\mathbf{x}_A) can be computed from the position of the other end of the train (\mathbf{x}_B) and the layout of the train track (\mathbf{T}) between the two points. The estimated position of receiver A is, then, a point along a three-dimensional curve \mathbf{T} , parametrized by ξ . This point, ξ_A is a function of the position of the reference receiver ξ_B , the track layout $\mathbf{T}(\xi)$, and the distance between the receivers along the train L :

$$\xi_A = \xi_B + L. \quad (2)$$

Similarly, the velocity at one end of the train (\mathbf{v}_A) has the same magnitude as at the other end of the train (\mathbf{v}_B), but a different direction. This direction is given by the track layout at ξ_A , where $\mathbf{T}(\xi_A) = \mathbf{x}_A$ and $\mathbf{1}_{TA}$ is the unit vector tangential to $\mathbf{T}(\xi)$ at $\xi = \xi_A$.

The kinematic constraint imposed by railway tracks enables the computation of accurate estimates \mathbf{x}_A , using only the position of receiver \mathbf{x}_B and the layout of the train track between them $\mathbf{T}(\xi)$. In this scenario \mathbf{x}_A must lie along the track, at a fixed distance L from

\mathbf{x}_B . This corresponds to a line integral:

$$\mathbf{x}_A = \mathbf{x}_B + \int_{\xi_B}^{\xi_B+L} \mathbf{T}(\xi) d\xi. \quad (3)$$

For the purpose of this paper, the train length L is assumed to be constant. During acceleration or deceleration of the train, its actual length might vary. This variation is proportional to the number of carriages and can become significant for very long trains; in such a case, the method needs to be adapted to accommodate a time-varying train length $L(t)$, possibly estimated from displacement sensors on the couplers between carriages.

The velocity of receiver A can be assumed to have the same magnitude as that of receiver B , with the direction of the velocity vector given by the along-track unit vector $\mathbf{1}_{TA}$:

$$\mathbf{v}_A = |\mathbf{v}_B| \mathbf{1}_{TA}. \quad (4)$$

Constrained GNSS Positioning

The standard GNSS position solution, as described in [2], can be adapted to accommodate the kinematic constraint imposed by a railroad track, as defined above by $\mathbf{T}(\xi)$. The resulting position solution will lie on the curve parametrized by \mathbf{T} , while only two satellites are needed as ranging sources with two states to be estimated: ξ and the clock bias b_u .

In the constrained system the pseudorange equation can be rewritten to replace the user position in three dimensions x_u with the track map \mathbf{T} evaluated at the along-track location ξ_u . The pseudorange $\rho^{(k)}$ between the user and satellite k becomes a function of ξ_u and b_u . The equation for the pseudorange (??) can be found at the top of the next page.

Redefining the pseudorange also requires a new definition of the Jacobian matrix, which is different from the conventional geometry matrix. The conventional geometry matrix has four entries in each row, three corresponding to the line-of-sight vector $\mathbf{1}^{(k)}$ and a 1 to account for the common clock bias. Taking the partial derivative of $\rho^{(k)}$ with respect to ξ_u and b_u results in a constrained geometry matrix:

$$G_c = \begin{bmatrix} \dots & \dots & \dots \\ \mathbf{1}^{(k)} \cdot \mathbf{1}_T(\xi) & 1 & \dots \\ \dots & \dots & \dots \end{bmatrix}. \quad (6)$$

Note that the new matrix G_c contains two elements for each satellite: the component of the line-of-sight vector, projected into the direction tangential to the track as given by the unit vector $\mathbf{1}_T(\xi)$, and the

$$\rho^{(k)}(\xi_u, b_u) = \sqrt{(x^{(k)} - T_x(\xi_u))^2 + (y^{(k)} - T_y(\xi_u))^2 + (z^{(k)} - T_z(\xi_u))^2} + b_u + \varepsilon^{(k)}. \quad (5)$$

component of the user clock bias. In consequence, two satellite signals are sufficient to provide a position estimate if \mathbf{T} is known.

The rest of the procedure for obtaining the constrained position solution follows the same mechanics as for the unconstrained solution, as described in [2]. Until convergence we compute expected measurements, compare difference them from the actual measurements and multiply by the pseudoinverse of G_c to obtain a new position guess.

Predicting Code Phase and Doppler Frequency

For the purposes of this paper we consider two fundamentally different ways of computing code phase and carrier frequency predictions, we refer to them as absolute and incremental. In the absolute method, the position and velocity of the aided receiver are explicitly computed, in order to then calculate the predicted quantities. In the incremental method, the quantities of interest are computed in relation to a different receiver that is currently locked onto the satellite signal.

Absolute Computation

One way of predicting the code phase ($\hat{\Phi}$) and carrier frequency (\hat{f}) of a satellite signal at a given receiver A is to compute the relative distance of the receiver to the satellite, as well as the relative velocity. Essentially, the code phase at the receiver is the distance between receiver and satellite, modulo the length of the code Λ . Similarly, the frequency of the received signal is offset from the transmission frequency by the relative velocity between satellite and receiver, divided by the wavelength of the carrier.

Given an estimate for the position $\hat{\mathbf{x}}_A$ of a GNSS receiver A , the position $\mathbf{x}^{(k)}$ of satellite k and the corresponding clock biases \hat{b}_A and $b^{(k)}$, as well as the receiver integration time Δt , the predicted code phase at receiver A is:

$$\hat{\Phi}_A^{(k)} = \left\lceil \frac{1}{c} \left[\|\mathbf{x}^{(k)} - \hat{\mathbf{x}}_A\| - (b^{(k)} - \hat{b}_A) \right] \right\rceil$$

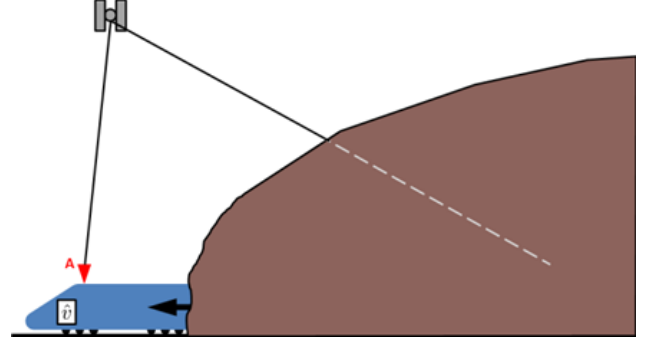


Figure 4: As a train exits a tunnel, its GNSS receivers may need to acquire signals from a different set of satellites than was visible before entering the tunnel.

$$+ \left(\beta \hat{f}_A[t]_{\mu s} + \alpha \right) \Big] \Big]_{\Lambda}. \quad (7)$$

The terms represented by β and α model the effect of a Doppler stretching of the code signal and an offset due to the electrical path from antenna phase center to correlator. Both terms can be calibrated ahead of time. The operator $[\]_{\mu s}$ indicates that only the time since the last chip transition (chip duration: 1 μ s). For the scope of this paper, the Doppler effect was modeled as an additive term. Such a model is accurate enough for short-term predictions, over the span of a few tens of seconds. As an item of future work, this model will have to be adapted to reflect a multiplicative term that better reflects the Doppler effect.

The predicted carrier frequency for that same receiver can be computed from the line-of-sight component of the relative velocity between receiver and satellite:

$$\hat{f}_A^{(k)} = \frac{(\hat{\mathbf{v}}_A - \mathbf{v}^{(k)}) \cdot \mathbf{1}^{(k)}}{\lambda}, \quad (8)$$

$$\mathbf{1}^{(k)} = \frac{\hat{\mathbf{x}}_A - \mathbf{x}^{(k)}}{\|\hat{\mathbf{x}}_A - \mathbf{x}^{(k)}\|}.$$

Incremental Computation

In contrast to the absolute method, the incremental method computes code phase and carrier frequency predictions relative to another receiver. It is assumed that the relative position \mathbf{X}_{AB} of the two receivers is known, as well as the position and velocity of the reference receiver B and the layout of the track $\mathbf{T}(\xi)$ at all times until just before receiver A acquires the

satellite signal.

The advantage over the absolute method lies in that it allows for a simpler computation, as it requires fewer parameters, particularly for the code-phase prediction.

The delay on receiver A (labeled τ_A) will be similar to that on receiver B (i.e. τ_B), save for a differential $\Delta\tau$:

$$\tau_A^{(k)} = \tau_B^{(k)} + \Delta\tau.$$

This time differential is due to a range differential $\Delta r = c\Delta\tau$, where c is the speed of light.

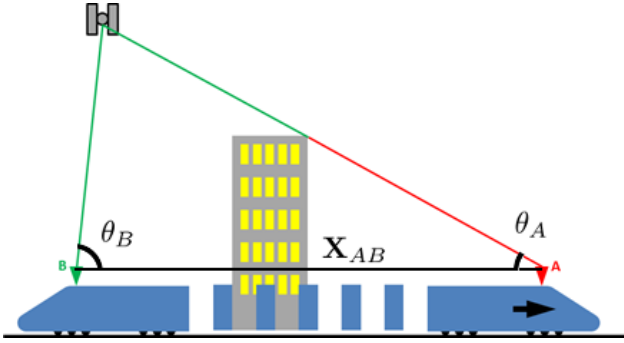


Figure 5: As receiver A re-emerges behind an obstacle, while receiver A is tracking satellite k , the tracking information from receiver B can be used to initialize receiver A seamlessly. The information needed for this process is the baseline between receivers, computed along the track $\mathbf{1}_{AB}$, and the angles between that baseline and the line of sight from each receiver to the satellite θ_A and θ_B .

From the geometry shown in Figure 5 the angles θ_A and θ_B can be determined from the known positions:

$$\cos(\theta_B) = \mathbf{1}_B^{(k)} \cdot \mathbf{1}_{AB},$$

$$\cos(\theta_A) = \mathbf{1}_A^{(k)} \cdot \mathbf{1}_{AB},$$

$$\sin(\theta_A) = \frac{\Delta r}{|\mathbf{X}_{AB}|}.$$

Here $\mathbf{1}_A^{(k)}$ and $\mathbf{1}_B^{(k)}$ are the unit vectors pointing from receivers A and B to satellite k , respectively. In addition, \mathbf{X}_{AB} is the baseline between the two receivers; and $\mathbf{1}_{AB}$ is the unit vector pointing along the baseline.

The predicted code phase at receiver A is the remainder of the sum of the code phase at receiver B plus the difference in line-of-sight distance Δr from the satellite to each receiver divided by the code length Λ .

For a given Δr the difference in code phase is:

$$\Delta\Phi = \left\lfloor \frac{\Delta r}{\Lambda} \right\rfloor, \quad (9)$$

and the difference in path length can be computed if the location of the two receivers is known:

$$\Delta r = \|\mathbf{x}_A - \mathbf{x}_B\| \frac{\cos(\theta_B)}{\cos(\theta_B - \theta_A)}. \quad (10)$$

From the above relationships, the expected code phase at receiver A becomes:

$$\hat{\Phi}_A = \left\lfloor \Phi_B + \frac{\|\mathbf{x}_A - \mathbf{x}_B\|}{\Lambda} \frac{\cos(\theta_B)}{\cos(\theta_B - \theta_A)} \right\rfloor. \quad (11)$$

The Doppler frequency on receiver B is simply: $\hat{f}_A = f_{\text{GNSS}} + \Delta f$, where Δf is the difference in frequencies between receiver A and B , due to Doppler shift:

$$\Delta f_A^{(k)} = \frac{(\mathbf{v}^{(k)} - \mathbf{v}_A) \cdot \mathbf{1}_A^{(k)}}{c} f_{\text{GNSS}},$$

and now \hat{f}_A and \hat{f}_B become:

$$\hat{f}_A = \frac{(\mathbf{v}^{(k)} - \mathbf{v}_A) \cdot \mathbf{1}_A^{(k)}}{c} (1 + f_{\text{GNSS}}),$$

$$\hat{f}_B = \frac{(\mathbf{v}^{(k)} - \mathbf{v}_B) \cdot \mathbf{1}_B^{(k)}}{c} (1 + f_{\text{GNSS}}). \quad (12)$$

Substituting $(1 + f_{\text{GNSS}})$ then yields the expression for the predicted frequency at receiver A , given the tracked frequency f_B at B and the direction of the railroad track at A and B . Thus we can have:

$$\hat{f}_A = \frac{(\mathbf{v}^{(k)} - \mathbf{v}_A) \cdot \mathbf{1}_A^{(k)}}{(\mathbf{v}^{(k)} - \mathbf{v}_B) \cdot \mathbf{1}_B^{(k)}} f_B. \quad (13)$$

The main advantage of the incremental method, compared to the direct method, is that it does not require explicit calibrating of the parameters α and β in equation (7), but instead they are implicitly included in the Φ_B term of equation (11), as long as the receivers A and B are identical.

Simulation and Experiment

To prove the feasibility of Seamless Handover, we tested the methods in two different setups, at different levels of abstraction. One was a simulated GNSS signal, analyzed with a software receiver, to gain insight into how tracking variables need to be treated, for example as we transfer tracking from receiver B to receiver A in Figure 5. The other experiment was needed to determine whether the uncertainty in the estimates of $\hat{\Phi}$ and \hat{f} could be assumed to be small enough to allow for seamless handover.

Signal Level Simulation

To understand the effects of mis-acquisition, we study the behavior of the prompt output from the correlator. The plot in Figure 6 shows the output of a correctly decoded signal, a signal with a 100 Hz acquisition error in carrier frequency, and a signal with a 1.5 chip acquisition error in code phase.

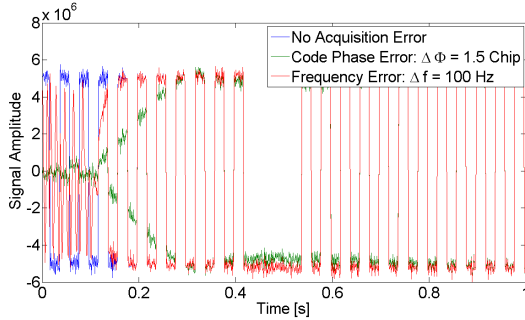


Figure 6: Three different responses at the “Prompt” correlator output of the DLL. The blue curve corresponds to a correct initialization, the green curve to an initialization error of 1.5 Chips, and the red curve to an initialization error of 100 Hz. The mis-initialized signals have a transient time during which the bits of the navigation message are decoded incorrectly, leading to transmission errors.

The tracking error in the mis-acquired signals reduces over time as the control loop, consisting of PLL and DLL, removes the disturbance. The correctly acquired signal displays distinct high and low values that will unequivocally be converted to a binary sequence, which we will assume as “correct” and use as a reference. Note that the significant difference between high and low reflects an SNR that is much higher than the effect of the initialization errors on Φ or f . By contrast, the mis-acquired signals will have decoding errors, as bit transitions are not as well-defined, or mis-timed. This will result in bit errors, during the transient, when the navigation message is decoded.

This setup motivates the use of bit errors in the decoding of the navigation message as an indicator of mis-acquisition. Conversely we assume that a signal decoded correctly, with no bit errors, indicates immediate lock onto the correct signal and, therefore, seamless handover of tracking. This assumption simplifies the task classifying acquisition as correct or incorrect and implicitly defines the duration of one data bit (20 ms) as epoch length for seamlessness.

Having defined zero bit error as the condition for successful acquisition motivates the experiment outlined

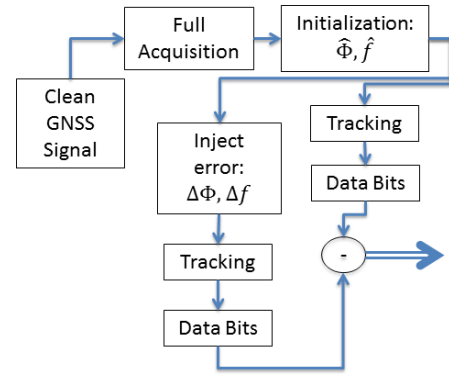


Figure 7: The correctness of a prediction of code phase and carrier frequency can be assessed by comparing the resulting bit sequence after the tracking loop. The assessment is based on the observation that a mis-initialized tracking loop will yield erroneous bit values during a transient time, until the tracking loop has locked onto the signal. This method gives a binary criterion for acquisition success or failure, which simplifies the search for the correct acquisition values compared to metrics based on the magnitude of the tracking errors.

in Figure 7. For each pair of $\Delta\Phi$ and Δf we compute the decoded bit sequence and compare that to the reference bit sequence when $\Delta\Phi = 0$ and $\Delta f = 0$.

Prediction of Code Phase and Carrier Frequency

The prediction methods described above were tested in a simulated setup, using a GNSS signal simulator [8] and a software-defined receiver [1]. The available data were appropriate for testing the absolute method, of equations (7) and (8). For this case, the quantities computed from a full, correlation-based search of the delay-Doppler space are accurate enough to be considered ground truth.

The predicted code phase was computed using (7) verified against the actual outputs of the DLLs of the software receiver. The plot in Figure 8 supports the claim that code phase can be acquired with an error below ± 0.2 chip lengths.

The frequency prediction, as computed by (8), was verified using the Doppler frequency measured at the PLL outputs, as a ground truth value. The plot of Figure 9 shows how the equation predicts the actual signal frequency to within ± 3 Hz.

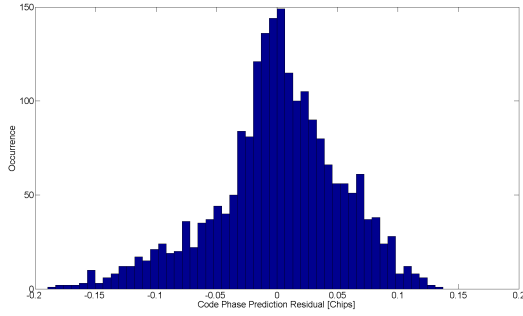


Figure 8: The prediction of the acquired code phase is verified against the frequency determined by the conventional method.

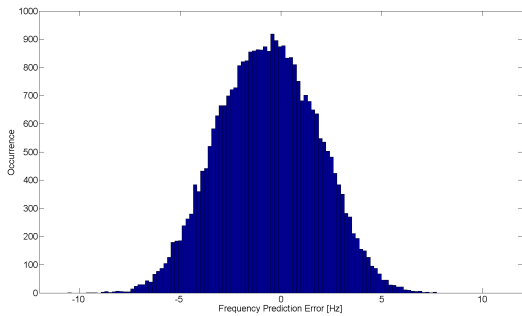


Figure 9: The prediction of the acquired signal frequency is verified against the Doppler frequency of the receiver.

Simulating the Propagation of Uncertainty

The goal of tracking handover is to provide the predicted $\hat{\Phi}$ and \hat{f} , which can be computed from equations (7) and (8). The following breakdown helps in quantifying the uncertainty behind the predictions, with the aim of determining whether seamless handover is feasible or not. For this simulation we assume a setup as in Figure 5, where the PVT solution at receiver A is computed from along-track integration from the reference receiver B .

The uncertainty on $\hat{\Phi}_A$ and \hat{f}_A is the result of the three steps in the prediction process, as each step adds uncertainty:

- The uncertainty in the position, velocity and time (PVT) estimates of the reference receiver B .
- The uncertainty introduced by along-track integration, using equation (3).
- The uncertainty in the computation of $\hat{\Phi}$ and \hat{f} .

This section addresses each of the steps and gives a conservative value for the total uncertainty in each predicted value.

Uncertainty in PVT

The first step in predicting $\hat{\Phi}$ and \hat{f} is to compute the position of the reference receiver, using the one-dimensionally constrained solution proposed in equation (6). Using data collected from real hardware receivers the method is shown to work, in Figure 10. The standard deviation of the along-track positioning error is $\sigma_\xi \approx 2$ m and $\sigma_v = .1$ m/s.

$$\mathbf{T}(\xi_B) \sim \mathcal{N}(\mathbf{T}(\hat{\xi}_B), \sigma_\xi). \quad (14)$$

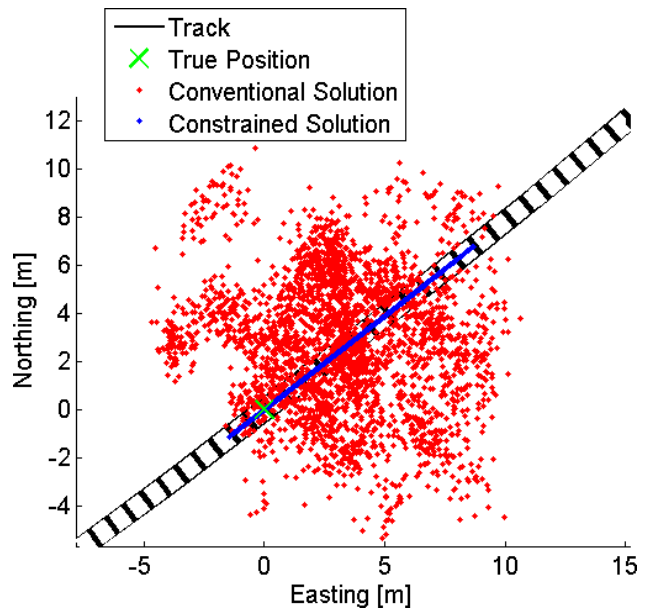


Figure 10: This experiment combines real GNSS measurement data with a real track layout. The red point cloud shows the 2-D positioning error of the unconstrained (conventional) GNSS solution, while the blue point cloud shows the error in the GNSS solution constrained to the track layout. Since the Jacobian does not change significantly within the extent of the error cloud, the errors in the constrained solution approximate the projection of the errors in the unconstrained solution, projected into the track map.

In terms of chip lengths and Doppler offsets, the above quantities translate as contributions to the uncertainty in estimating σ_Φ and σ_f . Namely: $\sigma_{\Phi, PVT} = 0.01$ chips and $\sigma_{f, PVT} = .5$ Hz.

Uncertainty in Along-Track Propagation

The track layout was similar to one provided by DLR [9]. The track data were provided as best estimates, but no ground truth was available. For that reason, the provided data were smoothed and interpolated at regular intervals to simulate ground truth. This simulated ground truth was degraded with random noise with a standard deviation of 1 m, which is significantly larger than is expected for map surveying errors, which can be assumed to be on the order of millimeters, according to [5] and [7].

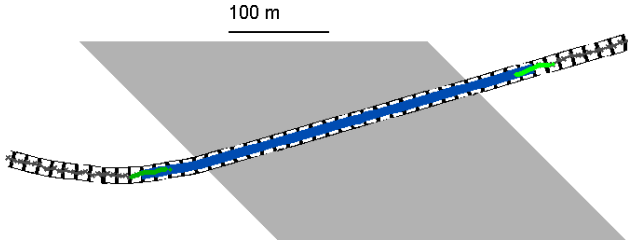


Figure 11: With the train assumed as traveling right to left, the leading receiver (left) is assumed to derive its position estimate from along-track integration relative to the reference receiver (right). The error cloud on the leading receiver appears very similar to the error cloud on the reference receiver, as the uncertainty in the PVT solution at the reference receiver dominates over the integration error: $\sigma_{\Phi, M} \ll \sigma_{\Phi, PVT}$

Propagating the position $\mathbf{T}(\xi_A)$ of receiver A along the train track, from the known position $\mathbf{T}(\xi_B)$ of receiver B will introduce an error that can be modeled as a Gaussian random walk. In that case the propagation error will be proportional to the surveying error and the number of surveyed points within the length of the train L . In the model used for Figure 11, the surveying error was taken to have a standard deviation of 1 m, which is conservative compared with available [5] and future [7] methods. In the simulations, the errors will not usually exceed a few meters, or a few tenths of a meter-per-second and so we model the contribution of the map to the prediction of σ_{Φ} and σ_f as: $\sigma_{\Phi, M} = 0.005$ chips and $\sigma_{f, M} = .05$ Hz.

Uncertainty in the Prediction of Code and Carrier

The the predictions from equations (7) and (8) are assessed for prediction performance. The results are depicted in Figures 8 and 9. From the Figures it can be seen that the code phase does not exceed 0.2 chip lengths and the frequency error follows a Gaussian

distribution with 95% of the error being within ± 5 Hz.

Furthermore, the data of Figure 8 support the view that adequate modeling of the Doppler effect in (7) would likely reduce the code phase prediction error to a Gaussian distribution with a standard deviation of .1 chips.

For the purpose of modeling the uncertainty in the prediction, we can thus assume: $\sigma_{\Phi, Pr} = 0.2$ chips and $\sigma_{f, Pr} = 5$ Hz.

Feasibility of Seamless Hand-Over

In order for a receiver (A) to seamlessly hand over tracking of a satellite (k) to another receiver (B), the code phase ($\hat{\Phi}$) and carrier frequency (\hat{f}) estimates must lie within the boundaries depicted in Figure 12. In a seamless handover, a GNSS receiver is able to lock on to a satellite from one epoch to the next using information provided by a different receiver that was able to track the satellite in the previous epoch.

Figure 12 shows the code-phase frequency plane and the color represents the error in decoding the navigation message. Black (i.e. zero) means that the navigation message was successfully decoded with no bit detection errors in the first 50 bits; white indicates that at least one bit error occurred in the decoding of the navigation message and, thus, a mis-acquisition occurred.

As can be seen in Figure 12, the basin in which the signal can be tracked without a transient is bounded by a code-phase error of roughly ± 5 chips and ± 50 Hz. These constraints are dramatically loosened if bit errors are tolerated in the startup phase of the tracking. On the other hand, reducing the noise bandwidth in either PLL or DLL will tighten the constraints.

Feasibility of the handover, therefore, will depend on the bandwidth of PLL and DLL and on the required sampling time. In the particular setup of this paper it is safe to assume that seamless hand-over is feasible, as the accuracy of the prediction lies within the boundaries of immediate tracking. The findings are summarized in Table .

The notion of seamlessly handing over satellite tracking from one GNSS receiver to another seems feasible in the light of the results summarized in Table . The table presents results from testing a tracking loop with a PLL noise bandwidth of 50 Hz and a DLL noise

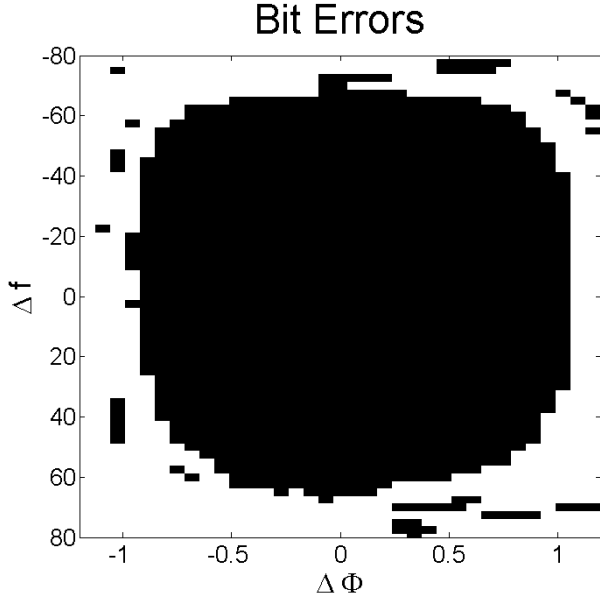


Figure 12: To achieve seamless handover, the acquisition method needs to provide accurate estimates of code phase and carrier frequency. The figure stems from acquiring PRN 22 with a receiver located at 34.7587° Latitude, 135.4273° Longitude. A black square indicates acquisition success for the corresponding injected $\Delta\Phi$ and Δf , a white square indicates a failed acquisition.

	PVT	Map	Pred	$\sqrt{\sum \sigma^2}$	Req
$\hat{\Phi}$.01 chip	.005 chip	.1 chip	.1006 chip	1 ch
\hat{f}	.5 Hz	.05 Hz	5 Hz	5.03 Hz	50 Hz

Table 1: Achieved accuracy in signal acquisition compared with the required accuracy for seamless handover. The total uncertainty is computed as the root-sum-square ($\sqrt{\sum \sigma^2}$) over the three different influences considered in the previous section: uncertainty due to PVT solution, due to map errors, and due to code and carrier predictions. The rightmost column represents the required accuracy for seamless handover, as illustrated in Figure 12.

bandwidth of 2 Hz. For each of the sources of uncertainty detailed in the previous section we list the contribution towards the total uncertainty, assuming that the errors are independent of each other and Gaussian distributed we model the uncertainty on the prediction of the code phase as:

$$\sigma_{\Phi} = \sqrt{\sigma_{P_{hi},PVT}^2 + \sigma_{P_{hi},M}^2 + \sigma_{P_{hi},Pr}^2}, \quad (15)$$

and similarly, the uncertainty on the predicted carrier

frequency will be:

$$\sigma_f = \sqrt{\sigma_{f,PVT}^2 + \sigma_{f,M}^2 + \sigma_{f,Pr}^2}, \quad (16)$$

Comparing the two right-most columns in Table we see that the total achievable uncertainty in prediction is smaller than the performance required for seamless handover of tracking.

Further Work

One compelling point to be addressed in the future is whether tracking handover will allow for a reduction in the noise bandwidth, both on the PLL and on the DLL in the tracking loop. As seamless handover allows accurate modeling of the code phase and carrier frequency, this knowledge can be leveraged in adequate design of GNSS receivers for railway applications. As modern GNSS receivers reduce the noise bandwidth in the tracking loop over time, an accurate prediction of the tracking state could allow the receiver to skip the intermediate steps (acquisition, progressive reduction of bandwidth) and go straight to the most narrow bandwidth available.

A second issue that remains for future work is the analysis of time granularity on seamless acquisition. It is likely that the appearance of the plots in Figure 12 would change in scale, but this change could potentially be very significant (like a change in the shape or over various orders of magnitude) or only minor (like a change in the outline of the zero-error region, as resolution increases). Since this represents, in some sense, an increase in sampling resolution, the impact is likely to be minor.

The third item that will have to be investigated is any benefit from predicting code phase and carrier frequency incrementally, as proposed in equations (11) and (13). This method will not require calibration of the constants required in the code phase prediction of the direct method and may yield more accurate predictions.

Summary

This paper has presented a method for exploiting geographic information to enable seamless handover of satellite tracking between multiple receivers on a train. The discussion has started with a look at the tracking loop in a GNSS receiver and how predictions of code phase and carrier frequency can reduce the

time to first fix. The prediction could be computed using any of a number of methods that have been previously proposed, but in a railway environment geographic information provides a compelling alternative, as trains move on tracks that are surveyed with much greater accuracy than a GNSS position fix could provide in real time.

Once the achievable performance is estimated, the paper compares that with the required accuracy in prediction that allows signal tracking to be handed over from one GNSS receiver to another without delay. It is established that the expected accuracy of the prediction methods presented earlier are sufficient to allow a general-purpose GNSS receiver to acquire lock on a satellite signal within a single epoch. This capability would, in turn, enable smooth transitions of tracking between different GNSS receivers on vehicles traveling at high speeds through cluttered environments, as long as at least one GNSS receiver has each satellite in view at any given time.

References

- [1] Kai Borre, Dennis Akos, Nicolaj Bertelsen, Peter Rinder, and Soren Holdt Jensen. *A Software-Defined GPS and Galileo Receiver: Single-Frequency Approach. A Single-Frequency Approach*. Birkhäuser Boston, 2007.
- [2] Pratap Misra and Per Enge. *Global Positioning System: Signals, Measurements and Performance Second Edition*. Massachusetts: Ganga-Jamuna Press, 2006.
- [3] Frank Stephen Tromp Van Diggelen. *A-GPS: Assisted GPS, GNSS, and SBAS*. Artech House, 2009.
- [4] Achim Hornbostel, Andriy Konovaltsev, and Pierre-Yves Dumas. MF/MC Receiver Performance Evaluation Under Nominal Interference Conditions for Definition of Receiver Parameter Space. In *Proceedings of the 2015 Global Navigation Satellite Systems Conference of the Institute of Navigation (ION GNSS 2015), Tampa, FL*, 2015.
- [5] Qijin Chen and Xiaoji Niu and Quan Zhang and Yahao Cheng . Railway Track Irregularity Measuring by GNSS/INS Integration. *Navigation*, 62(1):83–93, 2015.
- [6] J-M. Wiss, G. Barbu, Frosig, M. Schröder, C. Edwards, K. Walter, A. Filip, A. Sage, and S. Forsyth. Requirements of Rail Applications. Technical report, GNSS Rail User Forum, 2000.
- [7] Juliette Marais and Julie Beugin. Evaluation Method of GNSS-based Positioning Functions for Safety Applications in Operational Conditions . *Procedia - Social and Behavioral Sciences*, 48(0):806 – 815, 2012. Transport Research Arena 2012.
- [8] Spirent Communications. GNSS Engineer’s Handbook. Application Note DAN004-TM. Whitepaper, 2014.
- [9] Boubeker Belabbas, Anja Grosch, Oliver Heirich, Andreas Lehner, and Thomas Strang. Curvature Classification for Trains using Along-Track and Cross-Track Accelerometer and a Heading Rate Gyroscope. In *Proceedings of the European Navigation Conference*, 2013.